Smart Structures and Systems, *Vol. 35, No. 1 (2025) 29-38*
https://doi.org/10.12989/sss.2025.35.1.029

Deep learning prediction and evaluation of stability for piezoresistive behavior of the cement sensors

ZY Chen [1], Huakun Wu [2], Yahui Meng[**1] and Timothy Chen[*3]

[1] *School of Science, Guangdong University of Petrochem Technol, Maoming, Guangdong, China*
[2] *School of Computer Science, Guangdong Polytechnic Normal University, Guangzhou, Guangdong, China*
[3] *Division of Engineering and Applied Science, Caltech, CA 91125, USA*

(*Received June 3, 2024, Revised October 13, 2024, Accepted December 22, 2024*)

Abstract. Cement-based sensors are exposed to continuous dynamic loading and/or damage, degrading their sensing stability, nevertheless, predictions of long-term sensing stability have rarely been reported. Therefore, this study presents a deep-learning analysis combining experimental data and a LSTM model to predict the stability of long-term piezoresistivity. Related experiments are conducted, and the test results are used as training data. The simulations indicate that the parameters of the LSTM model have a notable effect on the predicted long-term piezoresistive sensing performances of the composites. By comparing the predictions with the experimental results, the validity of the proposed deep-learning approach is evaluated, and the following conclusions can be drawn from this study.

Keywords: AI & carbon nanotube; deep-learning; long-term cyclic loading; piezoresistive sensors; prediction and long short-term memory; recurrent neural network

1. Introduction

In the construction field, monitoring the long-term durability of structures throughout their service life is significant, and therefore considerable efforts have been made to monitor the soundness of structures efficiently (Chen *et al*. 2021, Dave and Purohit 2023). The advancement of smart materials has led to the development of cement-based sensors that utilize piezoresistive behavior to monitor structural health. The integration of deep learning techniques in predicting and evaluating the stability of these sensors represents a significant leap forward in civil engineering and material science.

Piezoresistive sensors change their electrical resistance in response to mechanical stress. This behavior is influenced by factors such as the microstructure of the cement, the type of aggregates used, and environmental conditions. Understanding these variables is crucial for enhancing sensor performance and reliability. Deep learning, particularly through artificial neural networks (ANNs), has been employed to model the complex relationships between the mechanical properties of cement and its piezoresistive response. Research has demonstrated that deep learning algorithms can effectively capture non-linear interactions, leading to improved predictive accuracy compared to traditional methods (Chen *et al*. 2007, 2010).

The stability of piezoresistive sensors under varying conditions is essential for their practical application. Studies have shown that deep learning models can be trained on large datasets to evaluate sensor performance under different loading scenarios and environmental stresses. Techniques such as convolutional neural networks (CNNs) and recurrent neural networks (RNNs) are particularly effective in analyzing time-series data from sensor outputs (Wang *et al*. 2023, Marquez *et al*. 2023, Koy and Çolak 2023).

Recent research has explored the use of transfer learning and data augmentation to enhance model robustness, especially in scenarios with limited training data. Additionally, Generative Adversarial Networks (GANs) have been utilized to simulate various loading conditions, enabling researchers to predict sensor behavior more accurately under diverse scenarios (Chen *et al*. 2022).

The incorporation of deep learning in the prediction and evaluation of the stability of piezoresistive behavior in cement sensors holds great promise for advancing structural health monitoring. Continued research in this area can lead to more reliable and efficient monitoring systems, ultimately contributing to safer infrastructure. Then, a deep learning-based LSTM model with three different input variables (time, MWCNTs content, and applied loading) and one output variable (fractional change in electrical resistivity, FCR) was adopted to predict the long-term piezoresistive sensing stability. In addition, numerical analysis was used to observe the suitable model parameters. Thereafter, the model was trained with 30% of the experimental data, and the remaining data were used to validate the predictions. Finally, the accuracy of the proposed model was evaluated in each cement-based sensor

*Corresponding author,
E-mail: t13929751005@gmail.com
**Co-corresponding author,
E-mail: mengyahui@gdupt.edu.cn

ISSN: 1738-1584 (Print), 1738-1991 (Online)

with different MWCNT contents.

2. Experimental piezoresistive sensing preliminary

The cement, aggregates, and piezoresistive materials were mixed in varying proportions (e.g., 0%, 1%, 3%, and 5% of carbon black by weight of cement). Dry ingredients were mixed thoroughly before adding water. The mixing was performed using a mechanical mixer for 10 minutes to ensure uniformity. Standard cube molds (50 mm × 50 mm × 50 mm) were cleaned and coated with a release agent. The mixed material was poured into molds and compacted to eliminate air bubbles. Samples were cured in a controlled environment (temperature: 20°C, humidity: 95%) for 28 days. Samples were immersed in water for the first 14 days, followed by air curing. The recorded electrical resistances are then converted to fractional resistance changes, as described in the previous study, using the following equation

$$FCR(\%) = \frac{R_t - R_0}{R_0} \times 100$$

where R_t denotes the electrical resistance at time t with compressive loading, and R_0 denotes the initial electrical resistance without an applied load.

The electrical resistivities and conductivities of the samples are shown in Fig. 1. Electrical resistivity is a measure of how strongly a material opposes the flow of electric current. It is an intrinsic property of materials. High conductivity indicates low resistivity and vice versa. Materials with high conductivity (like metals) allow electric current to flow easily, while materials with high resistivity (like insulators) do not. Factors Affecting Values: The resistivity and conductivity of a sample can be influenced by material composition and structural defects. The percolation threshold obtained in this study is equal to or less than that found in previous studies, indicating that the MWCNTs are well dispersed in the composites. Fig. 2 shows the piezoresistive sensing performance of the samples during the cyclic loading tests. The piezoresistive sensing performance of the samples was evaluated under cyclic loading conditions to assess their sensitivity, stability, and reliability in detecting changes in resistance due to mechanical strain. Based on the piezoresistive sensing performance results shown in Fig. 2, The results indicate that the samples exhibit promising piezoresistive sensing performance under cyclic loading conditions, making them suitable for applications in structural health monitoring and flexible electronics. Further optimization of material composition and structure may enhance their sensitivity and stability. The authors determined the 50 kN force for cyclic loading testing based on prior experimental data, material specifications, or design standards that suggest appropriate load levels for evaluating the performance and durability of the material under cyclic conditions. This force would have been chosen to ensure that the testing conditions effectively simulate realistic loading scenarios while remaining within the material's capacity to prevent premature failure.

The average gauge factor measured for the samples was found to be in the range of 5 to 15, indicating a moderate to high sensitivity to strain. The samples demonstrated a rapid response time, with resistance changes observable within milliseconds after the application of load. The samples were subjected to cyclic loads ranging from 0% to 5% strain. The resistance change was linear within this strain range, confirming the effectiveness of the piezoresistive mechanism. The samples exhibited stable performance over 1000 loading cycles, with minimal drift in resistance. A small hysteresis effect was observed, with a maximum deviation of approximately 2% in resistance during unloading compared to loading shown in Fig. 3.

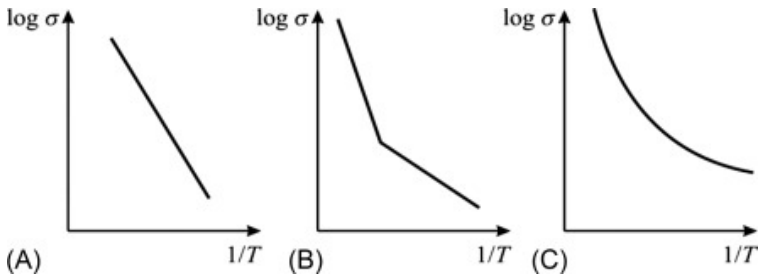

Fig. 1 The electrical resistivities and conductivities of the samples

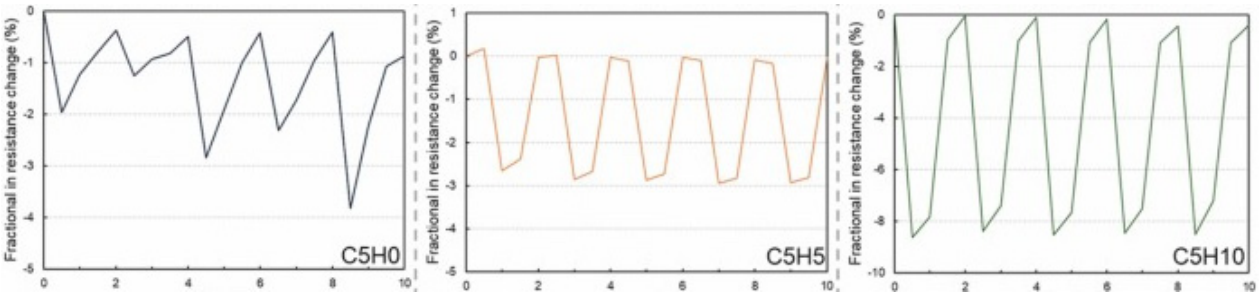

Fig. 2 Piezoresistive sensing performances of samples (a) C1; (b) C3; and (c) C5 during cyclic loading

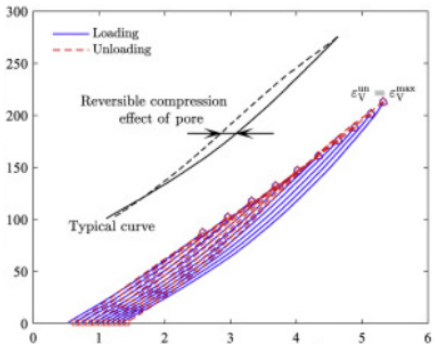

Fig. 3 Hysteresis effect observed with a maximum deviation of approximately 2%

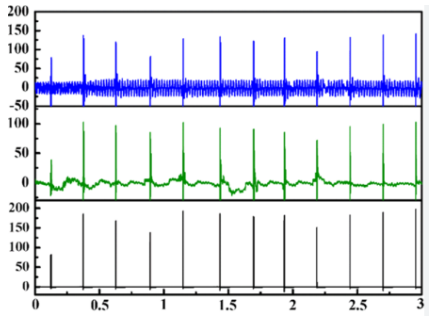

Fig. 4 Schematic description of response time expressed as peak shift and (b) peak shift values of samples obtained from the cyclic loading test

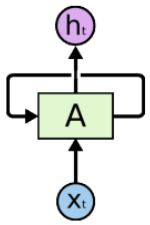

Fig. 5 Recurrent neural network

From Fig. 4, the sample with the highest MWCNT content has the fastest response when a compressive load is applied. From the piezoresistive sensing performance results, it can be found that the samples with MWCNT contents above the percolation threshold (i.e., 0.5 wt.%) are suitable for use as piezoresistive sensors because of their high sensitivity (FCR), good sensing stability (R2), and fast response (Peak shift).

3. LSTM model for prediction of long-term piezoresistive sensing performance

To assess the potential of the deep learning technique for time-dependent simulations of samples, a long short-term memory (LSTM) network is adopted in the present study. Recurrent neural networks (RNNs) are a basic concept in deep learning, and they consist of artificial neural network models with a structure continuously connected by nodes, similar to neurons. Here we provide the feedforward neural network with internal temporary storage and loop properties. The model used in the execution of each input data will not change, but at each moment The outputs will be affected by past calculations. After an output is generated, the output is copied and the copied value is sent back to the temporary storage of the recurrent neural network, as shown in Fig. 5. In the figure, the entire neural network structure is represented by A, and the input is xt, and the output generated by constructing A through the neural network is ht. When a recurrent neural network makes a decision, it considers both the current input and the output that has been learned based on past input.

The difference from feedforward neural networks is that RNN uses internal temporary states to generate actions for sequential inputs, which makes it quite feasible in non-segmented and connected problems, such as handwriting recognition or speech. identify. In other neural networks, all inputs are independent of other inputs, but in RNN, all inputs are related to each other, and there are loops in the structure. A neural network with a loop can be thought of as during the operation process, the output obtained during the previous execution will be copied and re-entered as input into the original neural network, so that past information can be passed on, so Fig. 5 can be equivalent to Fig. 6.

This chain-like network form clearly shows that the network has the same sequential nature as the input. In Fig. 6, the first input value of the sequence input x_0 is first input to the neural network. The output generated is h_0 used as the output and is also copied and stored in the temporary storage of the neural network. The next input x_1 enters the neural network. At the same time, the information temporarily stored in the neural network h_0 is also taken out as input and x_1 entered into the neural network together. The same step one value continues until the last piece of data input in the sequence x_t enters the neural network. The formula at the current stage can be expressed as formula (1)

$$h_t = f(h_{t-1}, x_t) \tag{1}$$

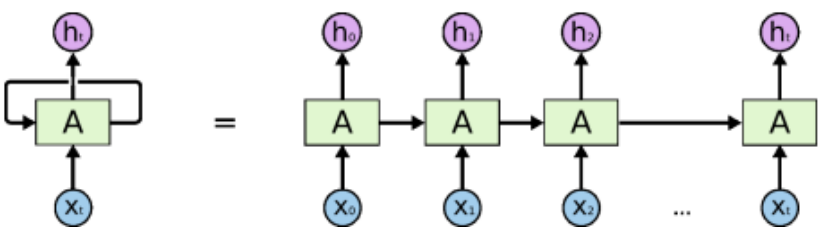

Fig. 6 A schematic diagram of disassembling the loops of a recurrent neural network

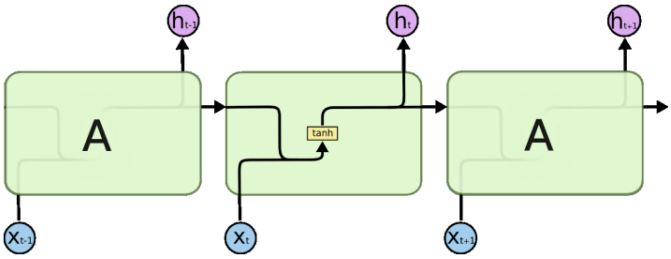

Fig. 7 Standard RNN architecture, using tanh as the excitation function as an example

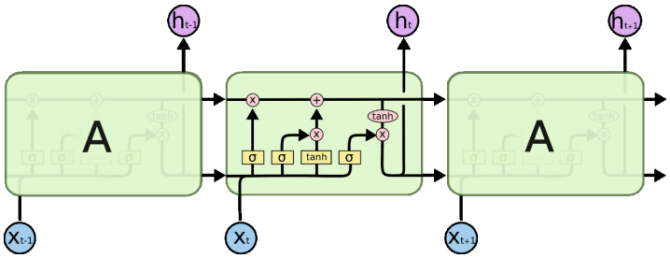

Fig. 8 The internal unit of LSTM is composed of four different functions, which influence each other

If there is an incentive function passed, it is assumed that the incentive function used is tanh, then the formula can be expressed as formula (2)

$$h_t = \tanh\left(W_{hh}h_{t-1} + W_{xh}x_t\right) \tag{2}$$

W represents the weight, h is the hidden vector of the single-layer neural hidden layer, W_{hh} is the weight of the previous hidden stage, W_{xh} represents the weight of the current input stage, falconan h is the excitation function, this function turns the neural network into a non-linear And the output is limited to [-1,1], and the output of the entire network can be expressed as Eq. (3), y_t which represents the output stage, W_{hy} which represents the weight of the output stage

$$y_t = W_{hy}h_t \tag{3}$$

The advantage of using RNN is that RNN can model data with sequential nature so that each sample can be related to previous samples. In addition, RNN can even be used in convolutional neural networks to increase the correlation between neighboring pixels. However, traditional RNN is not perfect. It has three main shortcomings. First, it may have gradient disappearance or gradient explosion problems during the execution process. Second, RNN is more difficult to train than other models., and finally, if tanh or relu is used as the excitation function, the input sequence cannot be too long. The LSTM method can effectively solve the above difficulties.

Long Short-Term Memory (LSTM) is a variant of traditional RNN. It is easier to remember past data in temporary storage than the original RNN, and the problem of gradient disappearance can also be solved by LSTM. When faced with a sequence of unknown length, LSTM can also effectively avoid time delays and effectively execute and make predictions or classifications. During the training process, LSTM uses error backpropagation, and in its network, there are three different gates, namely the input gate, the forget gate and the output gate. The single-layer neural network structure A of the traditional RNN in Fig. 6 can be represented in Fig. 7, while the schematic diagram using LSTM is shown in Fig. 8.

LSTM is similar to standard RNN and has the same characteristics of units being repeatedly connected, but its internal unit design is more complex than standard RNN and will interact with each other. In the middle square A in Fig. 8, each black line represents the direction of vector transmission, from an output node to another input place; the circular and elliptical parts are point operations, such as the phase of vectors. Addition or multiplication; the rectangular part represents the neural network layer that can be trained. If two lines intersect, it means they are connected, and if they diverge, it means the vector is copied and entered in two different directions.

First, we introduce the core concept of LSTM, which is to control the neural network through the switch of the gate. This process is called cell state. The unit state is like a conveyor belt, as shown in Fig. 9. It passes through the series connection of all neural networks and only encounters a few linear interactions during the conveyance process. Therefore, it is necessary to keep the information unchanged through this conveyor belt. Quite easy. LSTM cannot add or remove any information in the unit state, and can only control whether it is used through carefully specified gates.

The gate is a method of choosing whether to let data pass through, as shown in Fig. 10. It is composed of a neural network layer of sigmoid function and a dot multiplication operation. The S-shaped function layer will compress the output to between 0 and 1, which means what proportion of information needs to be allowed to pass through the gate in this layer. If the output is 0, it means that nothing will be allowed to pass. Otherwise, the output is 1. Let everything pass. There are three such gates in LSTM to protect and control the unit state.

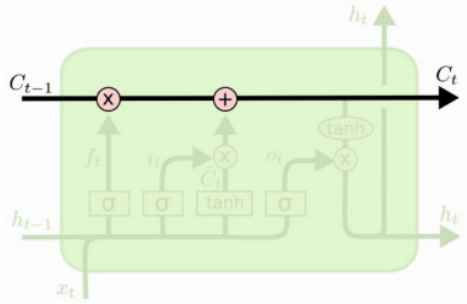

Fig. 9 Cell state in the LSTM architecture

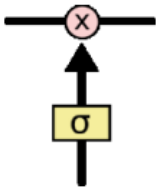

Fig. 10 Gate in LSTM

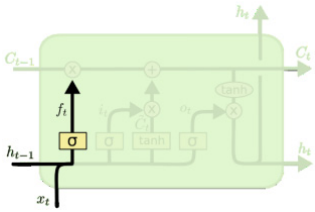

$$f_t = \sigma\left(W_f \cdot [h_{t-1}, x_t] \; + \; b_f\right)$$

Fig. 11 Schematic diagram of the forget gate in LSTM

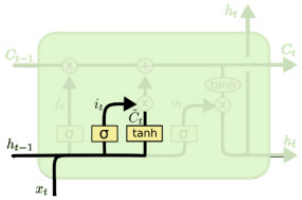

$$i_t = \sigma\left(W_i \cdot [h_{t-1}, x_t] \; + \; b_i\right)$$
$$\tilde{C}_t = \tanh(W_C \cdot [h_{t-1}, x_t] \; + \; b_C)$$

Fig. 12 How LSTM's new data enters the unit state

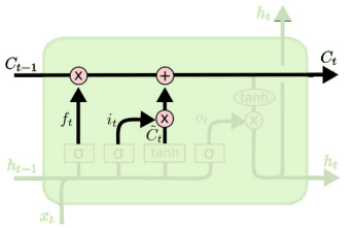

$$C_t = f_t * C_{t-1} + i_t * \tilde{C}_t$$

Fig. 13 Schematic diagram of LSTM inputting newly input information and forgotten gate information into the unit state

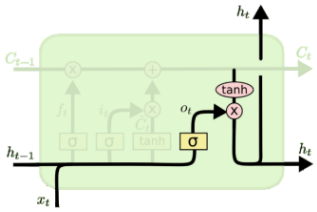

$$o_t = \sigma\left(W_o \; [h_{t-1}, x_t] \; + \; b_o\right)$$
$$h_t = o_t * \tanh\left(C_t\right)$$

Fig. 14 Schematic diagram of the final output of LSTM

The first step in LSTM is to decide what information is to be discarded from the unit state. This decision is made by a sigmoid layer called the forget gate. As shown in Fig. 11, h_{t-1}, x_t and C_{t-1} are each number received by the forget gate outputs a value between 0 and 1. 1 means to completely save the information, and 0 means to completely discard the information. For example, within the scope of English speech recognition, when predicting the next word based on the previous word, the gender information of the subject of the sentence may have been maintained in the unit state. At this time, the correct word can be used for subsequent pronouns. When we enter a new sentence and change the subject of the sentence, we must forget the gender information of the previous sentence.

The next step is to decide what new information to store in the unit state. As shown in Fig. 12, it is divided into two parts. The first is a sigmoid layer called the input gate layer. This layer determines which values will be updated. Then a tanh layer creates a vector of new values $\hat{C}_t$, which may later be accessed into the state. In the next action, the unit status will be updated based on the above two layers. Also speaking of the speech recognition system, when we want to add a new subject with a new gender, we will use this method to update and forget the old subject status.

The next step is to update the old unit state C_{t-1} to the new unit state C_t. First, multiply the past state that passed the forget gate f_t by the value of the unit state, and then add the new input value $i_t * \hat{C}t$. The size of this newly added value can be determined. In terms of the speech model, this stage is equivalent to completing the previously mentioned process of removing past gender characteristics and adding new information.

The last step is to decide what information to output. This output will be based on the previous unit state, but it will be a filtered version (Fig. 13). First run a sigmoid layer. The position of this sigmoid layer determines which part of the unit state is to be output. Then the unit state is passed through a tanh function to compress the passed value to between -1 and 1, and multiply it by sigmoid. The output of the gate makes the output position we get the position we want. Take the speech model as an example. When the model first sees the subject in the sentence, it predicts that it will output a verb next. So, after seeing the subject, the model first outputs whether the subject is singular or even. In this way, the subsequent output verb can be expressed using the correct grammar (Fig. 14).

3.2 Parametric analysis and piezoresistive predictions

In this study, the root-mean-square error (RMSE) is used to evaluate the performance of the proposed deep learning model. Fig. 15 displays the adopted dataset with 10,000 cycles for all the samples. The datasets include four variables: the quantity of MWCNTs, time, electrical

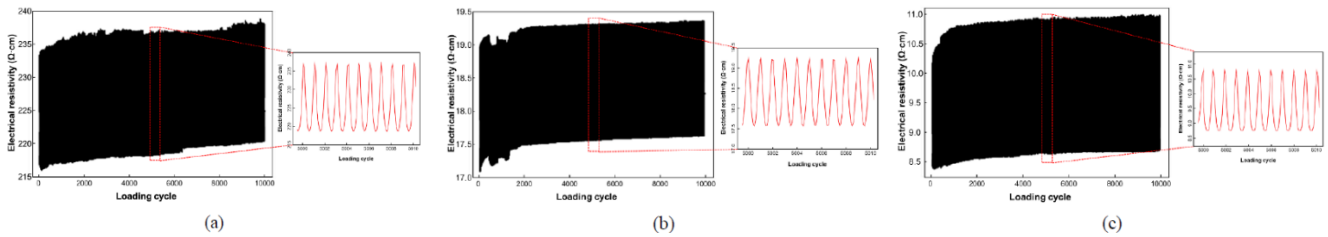

Fig. 15 Experimental results for adopted dataset with 10 000 cycles of samples (a) C1; (b) C2; and (c) C3

resistivity, and applied stress. Whereas the LSTM-based simulation parameters include the learning rate, number of epochs, and dropout ratio. Herein, the learning rate signifies how quickly the training process converges (Mohammadhassani *et al*. 2013, Meng *et al*. 2024a, b). The number of epochs means the number of executions, and in general, the accuracy improves as the number of epochs increases, however, increasing the number of epochs considerably increases the computational resources and time required.

Dropout is a learning method that arbitrarily deletes neurons, and users can arbitrarily set the ratio of neurons to be deleted (Tai *et al*. 2024). In general, the learning rate is an effective variable in solving the overfitting and under-fitting of prediction, in this study, it is fixed and applied to the experiment. A parametric study is conducted to examine the effects of these parameters with a control group and a comparison group. The results of these experiments are presented in Fig. 15, and the predictions are compared to the untrained experimental data to assess the predictive capability of the proposed deep learning-based model. The LSTM simulation is used to predict the FCR of the MWCNT/cement composites with various model parameters: the amount of training data, dropout ratio, and number of epochs.

The datasets are preprocessed for more accurate predictions and comparisons using MinMaxScaler. The C1 dataset is considered for an initial investigation of the model parameters.

Fig. 16 shows a comparison between the actual value (ground truth) and prediction for various dropout ratios. To examine the effect of dropout ratio, which prevents overfitting in the learning processes, a parametric study is conducted with various dropout values. Furthermore, to evaluate the effect of the weight parameter, three variables are set, as above. As the dropout ratio decreases, the prediction result is fitted more accurately. However, when the dropout ratio became extremely small, it is confirmed that the time almost doubled.

Among them, Table 1 shows the accuracy rate of Dataset1 using the reference point as the input data is the highest at 37.2%. In addition, the accuracy rate of Dataset1 with an allowable error of plus or minus one degree is also the best performance of 62.12%, although this is an excellent performance among all experimental data, but in practice it is impossible to perfectly extract the reference point from the test data, so the two data sets of Dataset2 and Dataset3 are used for prediction. When using 29 consecutive frames as the input of training data in Dataset2, the accuracy of the 3D convolutional neural network and the convolutional recurrent neural network is about 34.5%, which is about 2.5% higher than the multi-frame convolutional neural network, indicating that using RNN or 3D convolution kernels has better performance than simply using fully connected layers to string together feature vectors of different frames. When adding the allowable error $A \pm 1$, the accuracy of the other two models except CRNN is 59.39%, and CRNN is rare in this test. The accuracy of the allowable error is only about 57%. This is the only time in all data comparisons that the model performs significantly worse than other models. In Dataset3 using 9 consecutive frames, the accuracy of the convolutional recurrent neural network is the best, followed by the 3D convolutional neural network, and the worst performance is the Multi-frame convolutional neural network, among which Dataset3, which uses fewer consecutive frames, performs better than Dataset2 in convolutional recurrent neural networks, while 3D convolutional neural networks and Multi-frame convolutional neural networks perform worse than Dataset3. In the part of $A \pm 1$, the accuracy of CRNN after adding the allowable error exceeds 60%, while the performance of Multiframe convolutional neural network is the worst, just like its accuracy, only 56.31%. CRNN is required in the training and testing time of Dataset2, whether in Dataset2 or Dataset3, to use convolutional recurrent neural network, 3D convolutional neural network and Multi-frame convolutional neural network in one

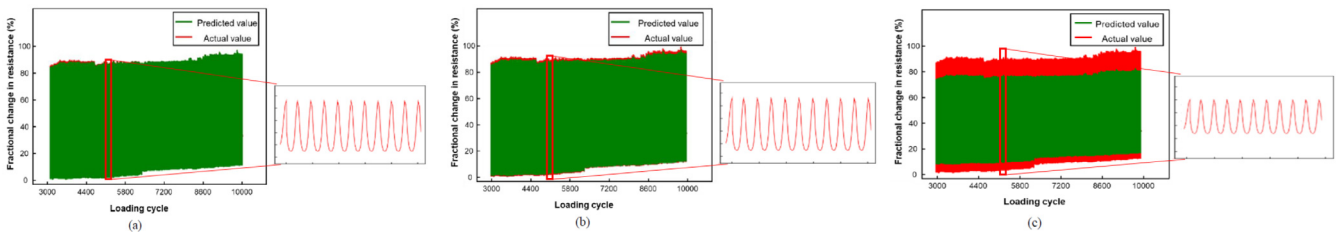

Fig. 16 Comparison of actual and predicted values with dropout ratios of (a) 0.1; (b) 0.3; and (c) 0.9

Table 1 Comparison of results without data enhancement

Training model	Data set	Accuracy	$A \pm 1$	Loss	Training time	Test time
Single-frame	Dataset1	**37.20%**	**62.12%**	1.7908	103 s	20 s
CRNN	Dataset2	**34.47%**	57.00%	1.7526	1174	401
	Dataset3	**35.84%**	**60.07%**	1.8110	355	115
3D CNN	Dataset2	34.47%	59.39%	1.8337	1221	406
	Dataset3	32.76%	59.39%	1.8945	373	124
Multi-frame	Dataset2	32.08%	59.39%	1.8561	1387 s	572 s
	Dataset3	30.72%	56.31%	1.8616	417 s	138 s

*$A_{\pm 1}$ is the accuracy rate of plus or minus 1 degree between the predicted angle and the label angle value

Table 2 Comparison of results using data enhancement

Training model	Data set	Accuracy	$A \pm 1$	Loss	Training time	Test time
Single-frame	Dataset1	**69.33%**	81.78%	1.0825	226 s	42 s
CRNN	Dataset2	64.88%	78.22%	1.2666	3310 s	1107 s
	Dataset3	**66.81%**	78.22%	1.1936	1220 s	407 s
3D CNN	Dataset2	**65.96%**	77.78%	1.0713	1458 s	485 s
	Dataset3	66.67%	78.07%	1.0409	504	167 s
Multi-frame	Dataset2	63.70%	76.89%	1.2298	3514 s	1130 s
	Dataset3	66.07%	77.93%	1.2555	819 s	265 s

*$A \pm 1$ is the accuracy rate of plus or minus 1 degree between the predicted angle and the label angle value

epoch. The time difference is not big, but the epoch required for 3D convolutional neural network and multi-frame convolutional neural network to achieve convergence is about 10 epochs, and the convolutional recurrent neural network requires 50 epochs. Convergence can be achieved only by about 10%.

After data enhancement of the training data, the accuracy rate is about 2 times higher, while the loss is reduced by about 2/3, which significantly improves the accuracy rate of the entire model. As can be seen from Table 2 below, in Dataset1, after using data enhancement, the accuracy rate increased significantly from the original 37.20% to 69.33%. This result is better than the result considering the allowable error when data enhancement was not used. In Dataset3, the best-performing training model is the convolutional recurrent neural network, and the worst is the Multi-frame convolutional neural network. However, the results obtained in terms of training time are the opposite. Each epoch convolution cycle for the time required by the neural network is almost 1.5 times that of the Multi-frame convolutional neural network, and it requires nearly 100 epochs to achieve effective convergence. In contrast, the Multi-frame convolutional neural network only requires a loss function within 10 epochs. can achieve convergence. The performance of the 3D convolutional network is between the above two. Regardless of the training time, testing time and accuracy, it is in the middle. The number of epochs required to achieve convergence is only slightly higher than that of the single convolutional neural network. Approximately 15 epochs.

In Dataset2, since the number of parameters of the input data is about three times that of Dataset3, the expected training time and testing time will be much higher. 3D convolutional neural network, convolutional recurrent network and Multi-frame convolution The training time of the recurrent network increases by about three times as does the number of parameters of the input data. In terms of accuracy, using more training data does not guarantee higher accuracy and smaller loss. In terms of accuracy, the accuracy of the three models of Dataset2 is lower than that of Dataset3, and in terms of loss, Only the method using Multi-frame convolutional neural network achieved a slight decrease. It is speculated that using more parameters but not achieving better accuracy may be because the data added is not frames near the label frame (reference point) but far away, and these frames affect the machine's judgment. Using the input data as Dataset2 and Dataset3 will not affect the number of epochs required to achieve convergence too much, indicating that the number of epochs required to achieve convergence has nothing to do with the input data, but is related to the architecture of the model itself. In Dataset2, the deep learning model that performs better in terms of accuracy or loss value is the 3D convolutional neural network. After data enhancement, the model with the best overall performance is the convolutional recurrent neural network of Dataset3. After considering the allowable error, the best-performing model is still Dataset1 using a single convolutional neural network at 81.78%. The other data have increased from the original 63.7% to 66.81% to 76.89% to 78.22%. Due to the accuracy after using data enhancement has reached more than 60%. Therefore, the improvement in accuracy after considering

the allowable error is not as obvious as the improvement in the overall accuracy after considering the allowable error for the data set without data enhancement.

4. Conclusions

The electrical resistivity decreases from 1279.1 to 59.5 Ω·cm as the embedded MWCNT content increases from 0.1 to 0.5 wt.%. For the piezoresistive sensing results, the sample with 0.5 wt.% of MWCNTs, which is within the range of the percolation threshold, shows the highest FCR of 17%. When a cyclic load is applied continuously, the FCR of the samples tends to be higher than that in the initial period. Samples with 0.5 wt.% of MWCNTs show the most stable long-term piezoresistive sensing behavior. The LSTM-based predictions are significantly affected by the model parameters, such as the quantity of training data, dropout ratio, and number of epochs. The optimal prediction results are obtained when the 30% of the total dataset is used for training, the dropout ratio is 0.3, and there are 50 epochs. To validate of the proposed deep learning approach, 30% of the total dataset is used to train the LSTM, and the piezoresistive sensing performance is predicted for the remaining 70%. The average RMSE is 0.02, and the average calculation time is approximately 1.14 h, which is 18% less than the time consumed by long-term piezoresistive sensing.

These findings are expected to contribute to predict the long-term sensing stability of cement-based sensors by considering the complex properties of cement, long-term behaviors, and mechanical-electrical relations. However, there have some imitations of the proposed model to apply in various types of cement-based sensors considering the external environmental conditions, thus, further studies will be carried out to improve the accuracy and mitigate the drawbacks of the proposed models. By combining experimental data, predictive modeling, and statistical analysis, we could effectively evaluate the long-term stability of the piezoresistive behavior of cement-based sensors. This comprehensive approach allows for informed decision-making regarding the reliability and durability of these sensors in practical applications.

In the experiment and results, we expect more details are required about the number of prepared and tested samples in the experiment for each category (C1, C3, and C5) and the configuration of setting them up. When the number of samples is presented, a discussion on to deal with discrepancies between results from different samples, and how the final experimental results are adopted would be suggested. Maximum compressive strength of the cubes measured or the stress-strain diagram drawn to analyze the material behavior under loading conditions are also suggested for further study.

References

Abolhasani, A., Pachenari, A., Razavian, S.M. and Abolhasani, M.M. (2022), "Towards new generation of electrode-free conductive cement composites utilizing nano carbon black", *Constr. Build. Mater.*, **323**, 126576. https://doi.org/10.1016/j.conbuildmat.2022.126576

Asteris, P.G., Apostolopoulou, M., Skentou, A.D. and Moropoulou, A. (2019), "Application of artificial neural networks for the prediction of the compressive strength of cement-based mortars", *Comput. Concrete, Int. J.*, **24**(4), 329-345. https://doi.org/10.12989/cac.2019.24.4.329

Bai, L., Han, P., Wang, J. and Wang, J. (2024), "Throughput Maximization for Multipath Secure Transmission in Wireless Ad-Hoc Networks", *IEEE Transact. Commun.*, **72**(11), 6810-6821. https://doi.org/10.1109/TCOMM.2024.3409539

Bhandari, M., Wang, J., Jang, D., Nam, I. and Huang, B. (2021), "A comparative study on the electrical and piezoresistive sensing characteristics of GFRP and CFRP composites with hybridized incorporation of carbon nanotubes, graphenes, carbon nanofibers, and graphite nanoplatelets", *Sensor*, **21**(21), 7291. https://doi.org/10.3390/s21217291

Chen, C.Y., Hsu, J.R.C., Cheng, M.H., Chen, H.H. and Kuo, C.F. (2007), "An investigation on internal solitary waves in a two-layer fluid: Propagation and reflection from steep slopes", *Ocean Eng.*, **34**(1), 171-184. https://doi.org/10.1016/j.oceaneng.2005.11.020

Chen, C.Y., Lee, W.I., Kuo, H.M., Chen, C.W. and Chen, K.H. (2010), "The study of a forecasting sales model for fresh food", *Exp. Syst. Appl.*, **37**(12), 7696-7702. https://doi.org/10.1016/j.eswa.2010.04.072

Chen, C.W., Chiang, W.L. and Hsiao, F.H. (2020), "Stability analysis of T–S fuzzy models for nonlinear multiple time-delay interconnected systems", *Math. Comput. Simul.*, **66**(6), 523-537. https://doi.org/10.1016/j.matcom.2004.04.001

Chen, C.W., Yeh, K. and Liu, K.F.R. (2022), "Adaptive fuzzy sliding mode control for seismically excited bridges with lead rubber bearing isolation", *Int. J. Uncertain. Fuzzi. Knowl.-Based Syst.*, **17**(05), 705-727. https://doi.org/10.1142/S0218488509006224

Dave, R. and Purohit, J. (2023), "Leveraging deep learning techniques to obtain efficacious segmentation results", *Arch. Adv. Eng. Sci.*, **1**(1), 11-26. https://doi.org/10.47852/bonviewAAES32021220

García-Macías, E., Castro-Triguero, R., Sáez, A. and Ubertini, F. (2018), "3D mixed micromechanics-FEM modeling of piezoresistive carbon nanotube smart concrete", *Comput. Methods Appl. Mech. Eng.*, **340**, 396-423. https://doi.org/10.1016/j.cma.2018.05.037

Graves, A., Mohamed, A.R. and Hinton, G. (2013), "Speech recognition with deep recurrent neural networks", 2013 IEEE International Conference on Acoustics, Speech and Signal Processing, May.

Guerra, V., Wan, C. and McNally, T. (2020), "Fused deposition modelling (FDM) of composites of graphene nanoplatelets and polymers for high thermal conductivity: A mini-review", *Funct. Compos. Mater.*, **1**(1), 1-11. https://doi.org/10.1186/s42252-020-00005-x

He, L., Pan, J., Hee, Y.S., Chen, H., Li, L.G., Panda, B. and Chow, W.T. (2024), "Development of novel concave and convex trowels for higher interlayer strength of 3D printed cement paste", *Case Stud. Constr. Mater.*, **21**, e03745. https://doi.org/10.1016/j.cscm.2024.e03745

Huang, X., Chang, L., Zhao, H. and Cai, Z. (2022), "Study on craniocerebral dynamics response and helmet protective performance under the blast waves", *Mater. Des.*, **224**, 111408. doi: https://doi.org/10.1016/j.matdes.2022.111408

Karim, F., Majumdar, S., Darabi, H. and Chen, S. (2017), "LSTM fully convolutional networks for time series classification", *IEEE Access*, **6**, 1662-1669. https://doi.org/10.1109/access.2017.2779939

Khalid, H.R., Choudhry, I., Jang, D., Abbas, N., Haider, M.S. and

Lee, H.K. (2021), "Facile synthesis of sprayed CNTs layer-embedded stretchable sensors with controllable sensitivity", *Polym*., **13**(2), 311. https://doi.org/10.3390/polym13020311

Koy, A. and Çolak, A.B. (2023), "The intraday high-frequency trading with different data ranges: A comparative study with artificial neural network and vector autoregressive models", *Arch*. *Adv*. *Eng*. *Sci*., **2**(3), 123-133. https://doi.org/10.47852/bonviewAAES32021325

Kratzert, F., Klotz, D., Brenner, C., Schulz, K. and Herrnegger, M. (2018), "Rainfall-runoff modelling using long short-term memory (LSTM) networks", *Hydrol*. *Earth Syst*. *Sci*., **22**(11), 6005-6022. https://doi.org/10.5194/hess-22-6005-2018

Kratzert, F., Klotz, D., Shalev, G., Klambauer, G., Hochreiter, S. and Nearing, G. (2019), "Towards learning universal, regional, and local hydrological behaviors via machine learning applied to large-sample datasets", *Hydrol*. *Earth Syst*. *Sci*., **23**(12), 5089-5110. https://doi.org/10.5194/hess-23-5089-2019

Li, H., Lu, H. and Li, Q. (2024a), "Numerical investigations of the influences of valve spool structure on the eccentric jet flow characteristic in high-pressure angle valves", *Energy*, **298**, 131378. https://doi.org/10.1016/j.energy.2024.131378

Li, M., Wang, L., Luo, C. and Wu, H. (2024b), "A new improved fractional Tikhonov regularization method for moving force identification", *Structures*, **60**, 105840. https://doi.org/10.1016/j.istruc.2023.105840

Liu, T., Zhao, G., Qu, B. and Gong, C. (2024), "Characterization of a fly ash-based hybrid well cement under different temperature curing conditions for natural gas hydrate drilling", *Constr*. *Build*. *Mater*., **445**, 137874. https://doi.org/10.1016/j.conbuildmat.2024.137874

Marquez, B.Y., Realyvásquez-Vargas, A., Lopez-Esparza, N. and Ramos, C.E. (2023), "Application of ordinary least squares regression and neural networks in predicting employee turnover in the industry", *Arch*. *Adv*. *Eng*. *Sci*., **2**(1), 30-36. https://doi.org/10.47852/bonviewAAES32021326

Meng, X., Lin, L., Li, H., Chen, Y. and Mei, H. (2024a), "Characteristics of streamer discharge along the insulation surface with embedded electrode", *IEEE Transact*. *Dielectr*. *Electr*. *Insul*., **31**(4), 2038-2044. https://doi.org/10.1109/TDEI.2024.3394833

Meng, X., Zhang, B., Cao, F. and Liao, Y. (2024b), "Effectiveness of Measures on Natural Gas Pipelines for Mitigating the Influence of DC Ground Current", *IEEE Transact*. *Power Delivery*, **39**(4), 2414-2423. https://doi.org/10.1109/TPWRD.2024.3406826

Mohammadhassani, M., Nezamabadi-Pour, H., Jumaat, M.Z., Jameel, M. and Arumugam, A. (2013), "Application of artificial neural networks (ANNs) and linear regressions (LR) to predict the deflection of concrete deep beams", *Comput*. *Concrete*, *Int*. *J*., **11**(3), 237-252. https://doi.org/10.12989/cac.2013.11.3.237

Nam, I.W., Souri, H. and Lee, H.K. (2016), "Percolation threshold and piezoresistive response of multi-wall carbon nanotube/ cement composites", *Smart Struct*. *Syst*., *Int*. *J*., **18**(2), 217-231. https://doi.org/10.12989/sss.2016.18.2.217

Nguyen, T.N., Yu, Y., Li, J., Gowripalan, N. and Sirivivatnanon, V. (2019), "Elastic modulus of ASR-affected concrete: An evaluation using Artificial Neural Network", *Comput*. *Concrete*, *Int*. *J*., **24**(6), 541-553. https://doi.org/10.12989/cac.2019.24.6.541

Nie, F., Chow, C.L. and Lau, D. (2022), "A review on multiscale modeling of asphalt: Development and applications", *Multisc*. *Sci*. *Eng*., **3**(3-4), 1-18. https://doi.org/10.1007/s42493-022-00076-x

Ongpeng, J., Soberano, M., Oreta, A. and Hirose, S. (2017), "Artificial neural network model using ultrasonic test results to predict compressive stress in concrete", *Comput*. *Concrete*, *Int*. *J*., **19**(1), 59-68. https://doi.org/10.12989/cac.2017.19.1.059

Shi, M., Hu, W., Li, M., Zhang, J., Song, X. and Sun, W. (2023), "Ensemble regression based on polynomial regression-based decision tree and its application in the in-situ data of tunnel boring machine", *Mech*. *Syst*. *Signal Process*., **188**, 110022. https://doi.org/10.1016/j.ymssp.2022.110022

Sun, Q., Wang, H., Liu, W., Zou, J., Ye, F. and Li, Y. (2024), "An Improved Stereo Visual-Inertial SLAM Algorithm Based on Point-and-Line Features for Subterranean Environments", *IEEE Transact*. *Vehicul*. *Technol*., 1-16. https://doi.org/10.1109/TVT.2024.3492388

Tai, S., Bu, C., Wang, Y.L., Yue, T., Liu, T., Liu, H.L. and Wang, L.X. (2024), "Identification of aircraft longitudinal aerodynamic parameters using an online corrective test for wind tunnel virtual flight", *Chinese J*. *Aeronaut*., **37**(9), 261-275. https://doi.org/10.1016/j.cja.2024.05.031

Wang, Y., Zhao, X. and Zhao, Y. (2020), "Piezoresistivity of cement matrix composites incorporating multiwalled carbon nanotubes due to moisture variation", *Adv*. *Civil Eng*., **2020**, Article ID 5476092. https://doi.org/10.1155/2020/5476092

Wang, Z., Wang, S., Wang, X. and Luo, X. (2023a), "Permanent Magnet-Based Superficial Flow Velometer With Ultralow Output Drift", *IEEE Transact*. *Instrum*. *Measur*., **72**, 1-12. https://doi.org/10.1109/TIM.2023.3304692

Wang, K., Chen, Z., Wang, Z., Chen, Q. and Ma, D. (2023b), "Critical Dynamic Stress and Cumulative Plastic Deformation of Calcareous Sand Filler Based on Shakedown Theory", *J*. *Marine Sci*. *Eng*., **11**(1), 195. https://doi.org/10.3390/jmse11010195

Wang, H., Zhang, Q., Fan, Z., Wang, G., Ding, P. and Wang, W. (2024a), "Towards an obstacle detection system for robot obstacle negotiation", *Indust*. *Robot*: *Int*. *J*. *Robot*. *Res*. *Applicat*., **51**(2), 236-245. https://doi.org/10.1108/IR-09-2023-0210

Wang, J., Bai, L., Fang, Z., Han, R., Wang, J. and Choi, J. (2024b), "Age of Information Based URLLC Transmission for UAVs on Pylon Turn", *IEEE Transact*. *Vehicul*. *Technolo*., **73**(6), 8797-8809. https://doi.org/10.1109/TVT.2024.3358844

Wang, J., Lin, S.Q., Tan, D.Y., Yin, J.H., Zhu, H.H. and Kuok, S.C. (2024c), "A Novel Method for Integrity Assessment of Soil-Nailing Works with Actively Heated Fiber-Optic Sensors", *J*. *Geotech*. *Geoenviron*. *Eng*., **150**(8), 04024063. https://doi.org/10.1061/JGGEFK.GTENG-11790

Wang, Z., Wang, K., Han, Q., Ni, J. and Wu, Z. (2025), "Crack imaging of underwater concrete components using interfacial waves and transducer array", *Mech*. *Syst*. *Signal Process*., **224**, 111998. https://doi.org/10.1016/j.ymssp.2024.111998

Xiang, Y., Wang, Z., Zhang, S., Jiang, L., Lin, Y. and Tan, J. (2024), "Cross-sectional performance prediction of metal tubes bending with tangential variable boosting based on parameters-weight-adaptive CNN", *Expert Syst*. *Applicat*., **237**, 121465. https://doi.org/10.1016/j.eswa.2023.121465

Xu, B. and Guo, Y. (2022), "A novel DVL calibration method based on robust invariant extended Kalman filter", *IEEE Transact*. *Vehicul*. *Technol*., **71**(9), 9422-9434. https://doi.org/10.1109/TVT.2022.3182017

Xu, B., Wang, X., Zhang, J., Guo, Y. and Razzaqi, A.A. (2022), "A novel adaptive filtering for cooperative localization under compass failure and non-gaussian noise", *IEEE Transact*. *Vehicul*. *Technol*., **71**(4), 3737-3749. https://doi.org/10.1109/TVT.2022.3145095

Xu, F., Bai, W., Zhang, J. and Jin, L. (2024), "The synthesis and application of MRI-fluorescence dual mode materials with absorption ability on quantitative analysis of malachite green", *Physica Scripta*, **99**(10), 105575. https://doi.org/10.1088/1402-4896/ad7d4a

Yadav, A., Jha, C.K. and Sharan, A. (2020), "Optimizing LSTM for time series prediction in Indian stock market", *Procedia*

Comput. *Sci*., **167**, 2091-2100. https://doi.org/10.1016/j.procs.2020.03.257
Yu, H., Wang, H. and Lian, Z. (2022), "An Assessment of Seal Ability of Tubing Threaded Connections: A Hybrid Empirical-Numerical Method", *J*. *Energy Resour*. *Technol*., **145**(5). https://doi.org/10.1115/1.4056332
Yu, S., Guan, D., Gu, Z., Guo, J., Liu, Z. and Liu, Y. (2024), "Radar Target Complex High-Resolution Range Profile Modulation by External Time Coding Metasurface", *IEEE Transact*. *Microw*. *Theory Techniq*., **72**(10), 6083-6093. https://doi.org/10.1109/TMTT.2024.3385421
Zhang, H., Wang, H. and Lian, Z. (2014), "Interconnected TS fuzzy technique for nonlinear time-delay structural systems", *Nonlin*. *Dyn*., **76**, 13-22. https://doi.org/10.1007/s11071-013-0841-8
Zhang, H., Wang, H. and Lian, Z. (2015), "Smart monitoring system with multi-criteria decision", *Smart Struct*. *Syst*., *Int*. *J*., **15**(6), 1583-1600. https://doi.org/10.12989/sss.2015.15.6.1583